

Molecular Gas and Star Formation in the SAURON Early-type Galaxies

Françoise Combes,^{1*} Lisa M. Young,^{2,3} Martin Bureau³

¹*Observatoire de Paris, LERMA, 61 Av. de l’Observatoire, 75014, Paris, France*

²*Physics Department, New Mexico Institute of Mining and Technology, Socorro, NM 87801, U.S.A.*

³*Sub-Department of Astrophysics, University of Oxford, Denys Wilkinson Building, Keble Road, Oxford OX1 3RH*

5 February 2018

ABSTRACT

We present the results of a survey of CO emission in 43 of the 48 representative E/S0 galaxies observed in the optical with the SAURON integral-field spectrograph. The CO detection rate is 12/43 or 28%. This is lower than previous studies of early-types but can probably be attributed to different sample selection criteria. As expected, earlier type, more luminous and massive galaxies have a relatively lower molecular gas content. We find that CO-rich galaxies tend to have higher H β but lower Fe5015 and Mgb absorption indices than CO-poor galaxies. Those trends appear primarily driven by the age of the stars, an hypothesis supported by the fact that the galaxies with the strongest evidence of star formation are also the most CO-rich. In fact, the early-type galaxies from the current sample appear to extend the well-known correlations between FIR luminosity, dust mass and molecular mass of other galaxy types. The star formation interpretation is also consistent with the SAURON galaxies’ radio continuum and FIR flux ratios, and their inferred star formation efficiencies are similar to those in spiral galaxies. It thus appears that we have identified the material fueling (residual) star formation in early-type galaxies, and have demonstrated that it is actively being transformed. Nevertheless, the lack of strong correlations between the CO content and most stellar parameters is compatible with the idea that, in a significant number of sample galaxies, the molecular gas has been accreted from the outside and has properties rather independent from the old, pre-existing stellar component.

Key words: galaxies: elliptical and lenticular, cD — galaxies: evolution — galaxies: ISM — galaxies: structure — Radio lines: galaxies.

1 INTRODUCTION

Over the last twenty years, growing evidence has accumulated that early-type galaxies (E/S0s) have detectable amounts of cold gas, sometimes settled in a disc, and recent star formation (e.g. Bregman, Hogg & Roberts 1991; Hogg, Roberts & Sandage 1993; Ferrari et al. 1999; Morganti et al. 2006). Many E/S0s also show photometric and kinematic evidence of central stellar discs (e.g. Bender 1988; Nieto, Capaccioli & Held 1988), the presence of which correlates with both nuclear and global properties (e.g. Nieto, Bender & Surma 1991; Faber et al. 1997). Similarly, many E/S0s show evidence for so-called kinematically decoupled cores (KDCs), i.e. kinematically misaligned central components (e.g. Franx, Illingworth & Heckman 1989; Emsellem et al. 2004). These point to the accretion of external material, question the importance of dissipation, and

may indicate triaxial figures. However, for both central discs and KDCs, the connection between stellar and gaseous components remains unclear.

Discs in ellipticals can form simultaneously with their host, from the major mergers of gas-rich galaxies. There has been evidence for this scenario for a number of years (see Hibbard et al. 1994 for NGC 7252; van Gorkom & Schiminovich 1997 for a review), and recent numerical simulations illustrate how the disc formation may happen (e.g. Barnes 2002; Naab, Jesseit & Burkert 2006). In those mergers, roughly half the gas is quickly funneled to the center, some causing a burst of star formation and much settling in a high surface density, mostly molecular central disc (e.g. Bournaud, Jog & Combes 2005). The other half is ejected to large distances but remains bound to the merger remnant (the new galaxy). This high angular momentum diffuse gas eventually falls back and may settle into a more extended, large-scale disc.

Alternatively, some gas could come from stellar mass

* E-mail: francoise.combes@obspm.fr

loss from evolved stars, and Sage & Welch (2006) recently proposed that essentially all the molecular gas found in the center of S0s does come from (internal) stellar mass return, while the atomic gas (HI) mainly originates from external sources (merger-driven infall, captured dwarfs, regular cold accretion, etc). Nevertheless, it is as yet not understood why early-type galaxies only possess $\sim 10\%$ of the gas expected from internal mass loss (e.g. Ciotti et al. 1991).

There have been several CO emission surveys of early-type galaxies (e.g. Lees et al. 1991; Wiklind, Combes & Henkel 1995; Sage, Welch & Young 2006; see also the compilation by Bettoni, Galletta & Garcia-Burillo 2003), revealing that early-types are not always devoid of gas, and can even show a substantial amount of CO emission. Young (2002, 2005) mapped CO emission in seven Es, revealing regularly rotating molecular discs in all of them. She showed that these gas discs should be forming stellar discs with approximately the same size and mass as typically observed in Es (e.g. Seifert & Scorza 1996; Scorza et al. 1998; Emsellem et al. 2004). Unfortunately, at the present, we know of no E/S0 galaxy with appropriate data to establish a direct causal link between the molecular gas and the stellar disc (or KDC). Integral-field spectroscopy is by far the best tool to study those decoupled components, but there is simply no overlap between the existing CO and integral-field samples. The recently completed **SAURON** survey, however, offers a unique opportunity to reverse this trend.

Using a custom-designed panoramic integral-field spectrograph (Bacon et al. 2001), the **SAURON** team have mapped the stellar kinematics of a large representative sample of early-type galaxies in the North (see de Zeeuw et al. 2002 for the sample definition and preliminary results). Both the quantity and quality of these data represent tremendous improvements over previously available observations of E/S0s. Contrary to expectations, most galaxies show evidence of kinematic subcomponents which can be uniquely identified and characterised with the new integral-field maps. Kinematic misalignments, twists, dynamically cold subcomponents, and KDCs are all common (Emsellem et al. 2004). Roughly half of **SAURON** E/S0s show kinematic evidence of a central disc.

In addition to the stellar distribution and kinematics (I , V , σ , h_3 and h_4 ; Emsellem et al. 2004), **SAURON** simultaneously maps the ionised-gas distribution and kinematics ($H\beta$, [O III] and [N I] lines; Sarzi et al. 2006), as well as the age, metallicity and overabundance of the stellar populations (through the $H\beta$, Mgb , Fe5015 and Fe5270 line-strength indices; Kuntschner et al. 2006). The central stellar discs and KDCs are often accompanied by ionised-gas discs, but not always. Similarly, while most appear old, not all are. This wealth of information is, however, not yet assembled into a complete picture of the current state and formation history of these discs and KDCs.

To better understand the varied phenomena seen in the stellar and ionised-gas data, a detailed comparison with molecular gas is warranted. As only a few **SAURON** early-type galaxies had a CO detection, we recently carried out a single-dish CO survey of most **SAURON** E/S0s using the IRAM 30 m telescope. The results are presented and discussed here. Section 2 presents the details of our observations as well as literature data, while Section 3 summarises

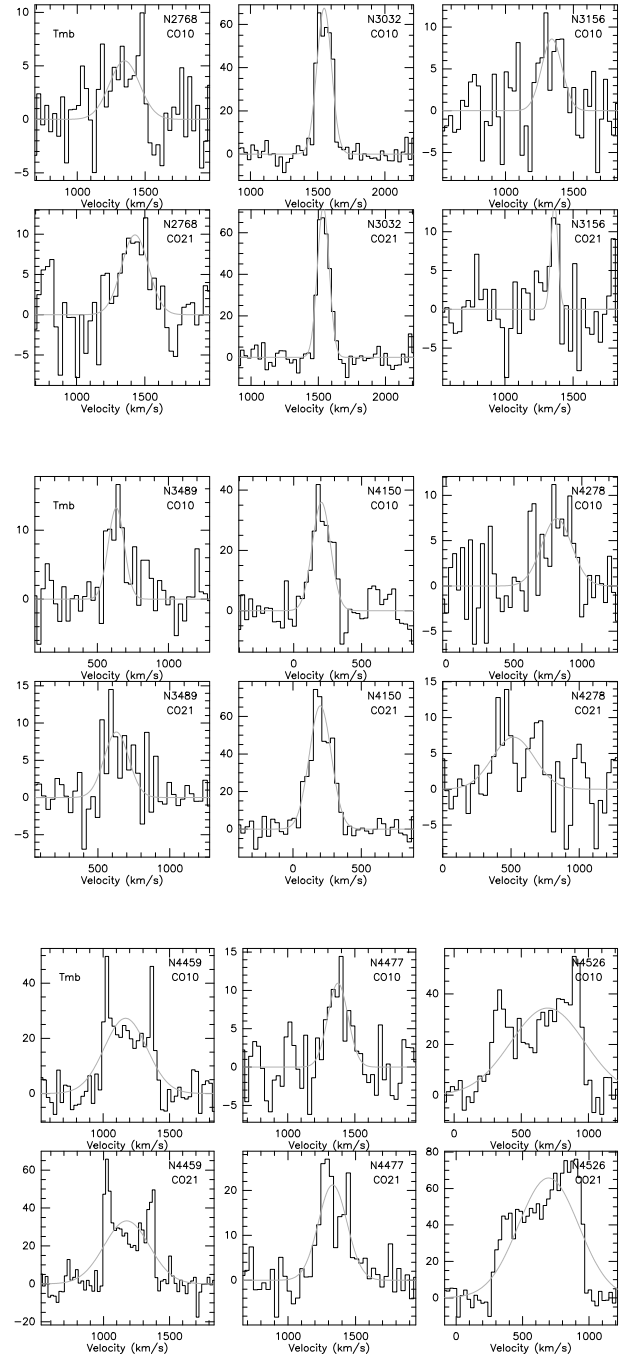


Figure 1. CO(1-0) and CO(2-1) IRAM 30 m spectra of the galaxies detected. The spectra have been binned to 30 km s^{-1} and the scale is T_{mb} in mK. Gaussian fits are overlaid (see § 2.1).

the basic results. Correlations with various physical quantities derived from **SAURON** and other sources are presented in Section 4, and the far infrared (FIR)-radio correlation is discussed in Section 5. We summarise our results and discuss their implications briefly in Section 6.

2 DATA

2.1 IRAM 30 m observations and data reduction

We simultaneously observed the CO(1-0) and CO(2-1) lines in the centre of the 43 early-type galaxies listed in Tables 1–2. Thirty-nine are from the **SAURON** representative sample of 48 E/SOs (de Zeeuw et al. 2002), and four were observed with **SAURON** for other purposes (e.g. Davies et al. 2001; Statler et al. 2004). We used the IRAM 30 m telescope at Pico Veleta, Spain, during April 2003 and April 2004. The beam FWHM is respectively 23'' and 12'' at the two frequencies. The SIS receivers were tuned in single side band mode to the redshifted frequencies of CO(1-0) at 2.6 mm and CO(2-1) at 1.3 mm. The observations were carried out in wobbler switching, with reference positions offset by 4' in azimuth. We used the 1 MHz back-ends with an effective total bandwidth of 512 MHz at 2.6 mm and the 4 MHz filterbanks with an effective total bandwidth of 1024 MHz at 1.3 mm.

We spent about 1–2 hours on each galaxy, resulting in a relatively homogeneous noise level of about 2–3 mK per (binned) 30 km s⁻¹ channel for all sources. The system temperatures ranged between 120 and 250 K at 2.6 mm, and between 300 and 500 K at 1.3 mm. The pointing was checked every 2 hours on a nearby planet or bright quasar. The temperature scale used is in main beam temperature T_{mb} . This was derived from antenna temperatures T_{a}^* by dividing by $\eta = B_{\text{eff}}/F_{\text{eff}} = 0.79$ at 2.6 mm and 0.57 at 1.3 mm, where B_{eff} and F_{eff} are respectively the beam and forward efficiencies.

Each spectrum was summed and reduced using linear baselines, and binned to 30 km s⁻¹ channels. Gaussian fits then yielded the peak intensities, central velocities, velocity FWHMs and integrated fluxes of the detected lines, listed in Table 1. Some of the lines are clearly not Gaussian in shape, but we have checked that integrating the area under the profiles yields consistent results within the uncertainties. The rms noise levels (1 σ after binning to 30 km s⁻¹) are listed for the non-detected galaxies in Table 2.

The total molecular hydrogen (H₂) mass was then computed, assuming the standard conversion ratio $N(\text{H}_2)/I(\text{CO}) = 3 \times 10^{20} \text{ cm}^{-2} (\text{K km s}^{-1})^{-1}$. Only the CO(1-0) line was used, and the H₂ mass corresponds to the 23'' beam, equivalent to 2.3 kpc at the average distance of our galaxies, $\langle D \rangle = 20$ Mpc. The H₂ masses may thus be underestimated if the molecular gas is more extended, but the beam does cover roughly one third of the **SAURON** field-of-view (33'' \times 41'' in low-resolution mode) and comparisons with optically determined parameters are justified on that basis. Furthermore, experience with interferometric imaging (e.g. Young 2002, 2005) suggests that little flux will be missed in most cases.

2.2 Comparison with previous observations

Among our 9 detections, some were already known. We confirm them here and in most cases improve the signal-to-noise ratio. NGC2768 was detected by Wiklind et al. (1995) with the IRAM 30 m, but with twice lower integrated intensities and line-widths, probably due to a pointing problem. NGC3032 was detected by several teams (Sage & Wrobel

1989; Thronson et al. 1989; Knapp & Rupen 1996) and our results are consistent with them. NGC3489 and NGC4150 were recently detected by Welch & Sage (2003) with the IRAM 30 m. They find a wider profile for NGC3489, but with a total bandwidth which is twice smaller, while NGC4150 is consistent. NGC4459 and NGC4526 were detected with smaller signal-to-noise ratios with the Kitt Peak 12 m telescope by Sage & Wrobel (1989). Their larger beam suggests that the CO emission is not extended much beyond our own 23'' beam. NGC3156, NGC4278 and NGC4477 are detected here for the first time.

Most of our upper limits are consistent with previous ones but improve them. Welch & Sage (2003) claim to detect NGC3384 in the CO(2-1) line with the IRAM 30 m, but nothing is detected in CO(1-0) either with IRAM or the Kitt Peak 12m. They however only have a narrow bandwidth of 650 km s⁻¹ at 1.3 mm, for a claimed line of zero-power width of 400 km s⁻¹, and there is the possibility of a baseline problem. With a bandwidth twice as large, our CO(2-1) spectrum is not consistent with their detection, and we consider NGC3384 as an upper limit in the rest of this paper.

2.3 Additional literature data

The representative **SAURON** sample of E/SOs is composed of the 48 galaxies listed in Table 3 (see also de Zeeuw et al. 2002). As stated above, we have observed with IRAM 43 galaxies previously observed with **SAURON**, of which 39 belong to this representative sample. We failed to observe the remaining 9 because of bad weather, but some have measurements in the literature. Once rescaled to our own conversion factor and distance (see de Zeeuw et al. 2002 for the latter), Watson, Guptill & Buchholz (1994) quote an H₂ mass of $5.2 \times 10^8 M_{\odot}$ for NGC2685, while Schinnerer & Scoville (2002) report $2.7 \times 10^7 M_{\odot}$. We adopt the more recent value. Wiklind & Henkel (2001) quote a molecular gas mass of $1.6 \times 10^7 M_{\odot}$ for NGC4550, and Welch & Sage (2003) $4.4 \times 10^6 M_{\odot}$ for NGC7457. Welch & Sage (2003) also provide an upper limit of $1.8 \times 10^8 M_{\odot}$ for NGC7332.

3 BASIC RESULTS

Figure 1 shows the 30 m spectra obtained in the CO(1-0) and CO(2-1) lines towards the 9 galaxies detected. The derived H₂ masses are listed in Table 3, together with relevant physical parameters against which the molecular content will be compared. For the non-detected galaxies, the quoted mass limits correspond to three times the statistical uncertainty in an integral over a 300 km s⁻¹ line width.

3.1 Excitation of molecular gas: the CO(2-1) to CO(1-0) ratio

The integrated CO(2-1)/CO(1-0) emission ratio is listed in Table 1 for all detected galaxies, as a first indicator of the excitation temperature of the gas. Since only one beam has been observed, it is not possible to compare the two lines with the same spatial resolution over the same region. The ratio is however generally quite low, ≈ 1.4 on average. In the case of a concentrated source, with the typical dense and optically thick molecular gas generally found in galaxy

Table 1. Parameters of the 9 early-type galaxies detected in CO.

Galaxy	$I_{(1-0)}$ (K km s ⁻¹)	$I_{(2-1)}$ (K km s ⁻¹)	$V_{(1-0)}$ (km s ⁻¹)	$V_{(2-1)}$ (km s ⁻¹)	$\Delta V_{(1-0)}$ (km s ⁻¹)	$\Delta V_{(2-1)}$ (km s ⁻¹)	Ratio	$T_{\text{mb}}(1-0)$ (mK)	$T_{\text{mb}}(2-1)$ (mK)
(1)	(2)	(3)	(4)	(5)	(6)	(7)	(8)	(9)	(10)
NGC2768	1.5 (0.28)	2.5 (0.47)	1421 (17)	1428 (23)	221 (51)	232 (49)	1.6 (0.43)	6.3 (2.5)	8.8 (3.5)
NGC3032	9.3 (0.30)	7.9 (0.23)	1549 (2)	1537 (2)	129 (4)	103 (3)	0.9 (0.04)	67.1 (5.1)	73.7 (5.3)
NGC3156	1.6 (0.37)	0.9 (0.23)	1341 (22)	1363 (10)	177 (35)	60 (18)	0.5 (0.19)	8.9 (3.8)	14.0 (3.5)
NGC3489	1.9 (0.30)	1.9 (0.33)	633 (10)	628 (21)	133 (28)	201 (45)	1.0 (0.24)	12.7 (2.5)	8.8 (1.8)
NGC4150	6.1 (0.49)	13.2 (0.47)	204 (7)	200 (3)	158 (14)	189 (8)	2.2 (0.20)	35.4 (5.1)	64.9 (3.5)
NGC4278	2.1 (0.41)	2.8 (0.60)	815 (27)	518 (41)	260 (59)	361 (76)	1.4 (0.39)	7.6 (2.5)	7.0 (3.5)
NGC4459	10.9 (0.48)	14.3 (0.51)	1169 (9)	1176 (8)	377 (16)	405 (15)	1.3 (0.07)	26.6 (8.9)	33.3 (7.0)
NGC4477	2.1 (0.33)	5.7 (0.47)	1374 (14)	1331 (11)	177 (31)	250 (23)	2.8 (0.50)	11.4 (2.5)	21.1 (5.3)
NGC4526	23.8 (0.76)	37.4 (0.72)	697 (2)	695 (5)	650 (23)	533 (11)	1.6 (0.06)	34.2 (3.8)	64.9 (8.8)

Columns: (1) Source name; (2)–(3) Integrated CO(1-0) and CO(2-1) emission; (4)–(5) Central velocity in CO(1-0) and CO(2-1); (6)–(7) Profile FWHM in CO(1-0) and CO(2-1); (8) Integrated CO(2-1)/CO(1-0) emission ratio; (9)–(10) Main beam peak temperature in CO(1-0) and CO(2-1). Uncertainties in each quantity are quoted in parenthesis. All galaxies are part of the **SAURON** representative sample (de Zeeuw et al. 2002).

nuclei (Braine & Combes 1992), we would expect a ratio of up to 4, the ratio of the beam areas for the two lines. The lower ratios observed suggest that the CO molecules are sub-thermally excited, and that the molecular gas density is relatively low on average.

3.2 CO detection rate

In the **SAURON** representative sample of 48 E/S0 galaxies, 43 galaxies have now been searched for CO emission. We detected 9 in both CO(1-0) and CO(2-1) emission and three have previous detections from the literature, corresponding to a detection rate of 28%. By construction, our sample contains half lenticular and half elliptical galaxies. Of the galaxies classed as ellipticals the detection rate is 2/20 (10%) and for lenticulars it is 10/23 (43%).

How does that compare to previous surveys? For lenticulars, the best comparison is with the survey of Welch & Sage (2003), which was a volume limited sample of non-Virgo cluster galaxies out to 20 Mpc. Their detection rate was 78%, much higher than ours. The difference may however lie in the fact that a volume-limited survey contains comparatively more small (and low-luminosity) galaxies, which tend to be richer in molecular gas (Lees et al. 1991; Sage et al. 2006). The **SAURON** sample was selected to uniformly populate planes of absolute magnitude M_B versus ellipticity ϵ , so its distribution in magnitude is approximately flat by construction, while the magnitude distribution of the complete sample from which it was drawn is much more skewed toward low-luminosity objects (see Fig. 1 in de Zeeuw et al. 2002). The median absolute magnitude of the **SAURON** sample is $M_B = -19.9$ whereas for the sample in Welch & Sage (2003) it is $M_B = -18.8$. The detection rate of Welch & Sage (2003) drops from 78% for the entire sample to 64% for galaxies brighter than $M_B = -18.8$, so our lower detection rate is roughly consistent with this trend.

There are probably several factors influencing the detection rates in the ellipticals. Knapp & Rupen (1996), Wiklind et al. (1995) and Lees et al. (1991) got detection rates of 30–40% for FIR-selected samples. Our detection rate is lower, most likely because the **SAURON** galaxies are not FIR-selected. However, we also have a lower detection

rate than Sage et al. (2006; 33%), who studied a volume-limited sample of ellipticals. The median M_B of their sample, -19.5 , is also a bit fainter than the median of the **SAURON** sample. Environment may also play a role, since again by construction half of the **SAURON** galaxies are in clusters. The effects of environment are however harder to gauge, since truly isolated early-type galaxies are rare, and we found no correlation between molecular gas content and environment (local galaxy number density; Tully 1988). Similarly, Kenney & Young (1989) found no deficiency in the molecular gas content of Virgo cluster spirals even though they are strongly deficient in atomic gas. At the moment, it nevertheless seems entirely plausible that differences between our results and previous works can be attributed mainly to different sample selection criteria.

3.3 Star formation tracers

In spiral galaxies the FIR emission is usually assumed to trace star formation activity. Therefore it is of interest to compare the FIR and molecular properties of the **SAURON** galaxies to those of star forming galaxies. A “bolometric” FIR flux is derived for each galaxy from the *IRAS* 60 and 100 μm fluxes,

$$FIR \equiv 1.26 \times 10^{-14} \text{ W m}^{-2} (2.58 S_{60\mu\text{m}} + S_{100\mu\text{m}}), \quad (1)$$

where $S_{60\mu\text{m}}$ and $S_{100\mu\text{m}}$ are measured in Jy. The total FIR luminosity is then $L_{\text{FIR}} = (FIR) 4\pi D^2$.

From the ratio of the *IRAS* 60 and 100 μm fluxes, we have derived dust temperatures assuming $\kappa_\nu \propto \nu$, where κ_ν is the mass opacity of the dust at frequency ν . The average dust temperature for the *IRAS*-detected **SAURON** galaxies is 30 ± 5 K. This is relatively low, indicating a low star formation density. By comparison, starburst galaxies have higher dust temperatures, ≈ 40 K or more (e.g. Sanders & Mirabel 1996).

Knowing the dust temperature T_{dust} and the 100 μm flux S_{100} , we can derive the dust mass as

$$\begin{aligned} M_{\text{dust}} &= 4.8 \times 10^{-11} \frac{S_\nu d_{\text{Mpc}}^2}{\kappa_\nu B_\nu(T_{\text{dust}})} M_\odot \\ &= 5 S_{100\mu\text{m}} d_{\text{Mpc}}^2 \{\exp(144/T_{\text{dust}}) - 1\} M_\odot, \end{aligned}$$

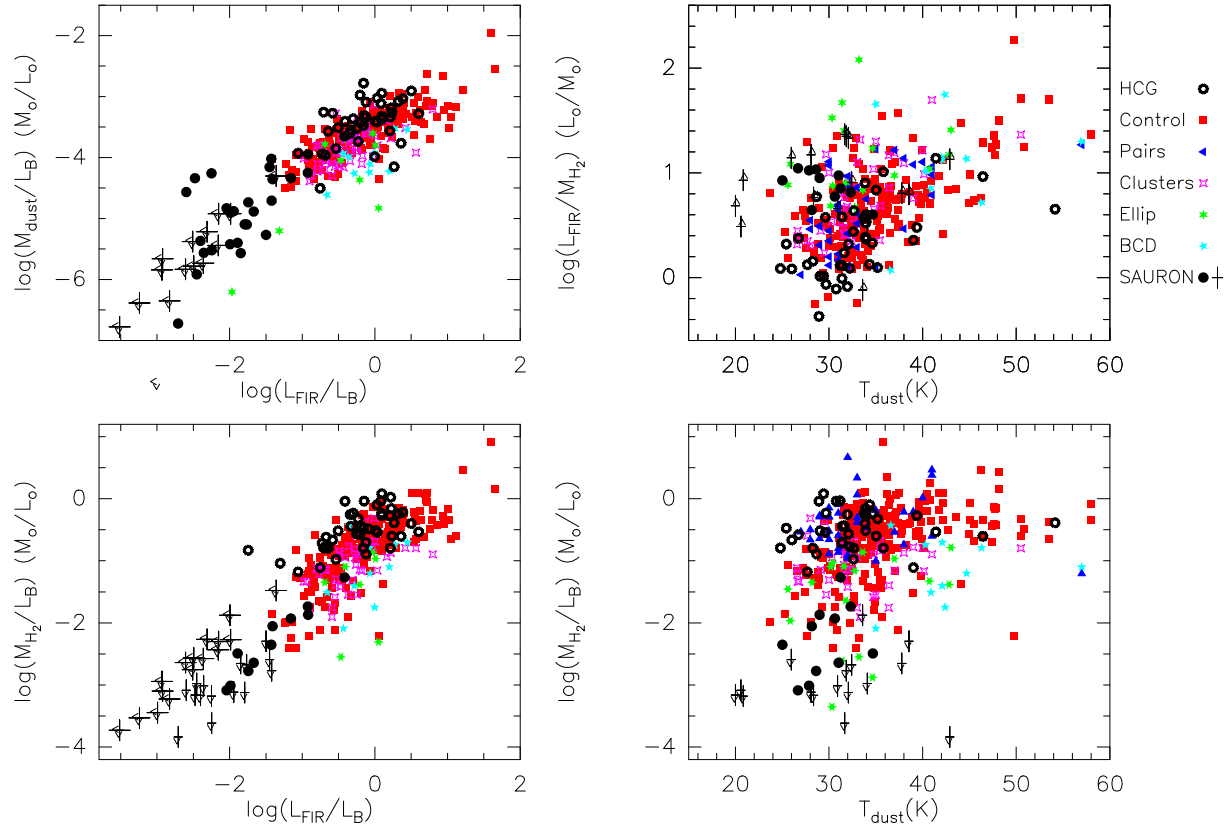


Figure 2. Comparison of the SAURON representative sample and other samples of galaxies observed in the CO line. The other samples are: HCG: Hickson Compact Group galaxies from Leon et al. (1998); Control: normal galaxies from Young et al. (1989, 1996), Solomon & Sage (1988), Tinney et al. (1990) and Sage (1993) (see Leon et al. 1998 for their definition); Pairs: binary galaxies (Combes et al. 1994) and starbursts (Sanders, Scoville & Soifer 1991); Clusters: galaxies in clusters (Casoli et al. 1991; Young et al. 1989); Ellip: elliptical galaxies from Wiklind et al. (1995); BCD: blue compact dwarf galaxies from Israel, Tacconi & Baas (1995) and Sage et al. (1992); SAURON: current sample (see de Zeeuw et al. 2002). **Top left:** Dust mass computed from IRAS fluxes (see text) versus FIR luminosity, both normalised by the blue luminosity. **Top right:** FIR luminosity to molecular mass (M_{H_2}) ratio, often used as a tracer of the star formation efficiency, as a function of dust temperature. Only *IRAS*-detected galaxies are plotted. **Bottom left:** M_{H_2} versus FIR luminosity, both normalised by the blue luminosity. **Bottom right:** M_{H_2} to blue luminosity ratio versus dust temperature. Only galaxies detected by *IRAS* are plotted.

where S_ν is the FIR flux measured in Jy, d_{Mpc} is the distance in Mpc, B_ν is Planck's function, and we use a mass opacity coefficient of $25 \text{ cm}^2 \text{ g}^{-1}$ at $100 \mu\text{m}$ (Hildebrand 1983). The presence of colder ($T \lesssim 20 \text{ K}$) dust could significantly change the derived dust masses but such an analysis would require additional millimeter and submillimeter continuum observations (e.g. Leeuw et al. 2004). For the current work such cold dust is neglected.

Figure 2 compares the dust and molecular content of the SAURON representative sample with various other samples studied in the literature. Those span a wide range of masses, metallicities and environments (field, group and cluster), with different star formation rates (starburst, quiescent) and different morphological types (elliptical, spiral, dwarf). The various samples are described in Leon, Combes & Menon (1998) and in Figure 2 itself.

The main correlations in Figure 2 are the well-known relations between the molecular content, dust content and FIR luminosity. The early-type galaxies from the present sample extend the relations toward low FIR-to-blue luminosity ratios L_{FIR}/L_B . Their molecular content normalised by the

blue luminosity is about 2 orders of magnitude lower than in normal spiral galaxies. In previous works, this dependency with type was not found to be so large, even though one of the essential characteristics of early-type galaxies is their low gas fraction (e.g. Casoli et al. 1991; Young & Scoville 1991). This result was generally attributed to metallicity effects, which influence the CO-to- H_2 conversion factor. Indeed, the content in molecular gas could in fact be lower in early-types, but this would not be noticed in the CO emission (when using a fixed CO-to- H_2 conversion factor) because of the compensating effect of a larger CO abundance per H_2 molecule. Early-type galaxies are in general more massive and, metallicity increasing monotonically with mass, also have higher metallicities. For a given decrease in molecular gas content, the CO emission is thus not dropping as fast. The present sample, due to the improved sensitivity of the telescope, extends the range in gas content to lower values, but it is not entirely clear why the molecular gas content dependence on morphological type is more acute than has been found in the past. The answer probably lies again in the different criteria used to select the targets (see § 3.2), but our results are also

Table 2. CO upper limits of the 34 non-detected early-type galaxies.

Galaxy	$T_{\text{mb}}(1-0)$ (mK)	$T_{\text{mb}}(2-1)$ (mK)	D (Mpc)	$\theta_{(1-0)}$ (kpc)	$\theta_{(2-1)}$ (kpc)
(1)	(2)	(3)	(4)	(5)	(6)
NGC0474	2.5	3.5	31.62	3.53	1.84
NGC1023	2.5	3.5	10.28	1.15	0.6
NGC2549	3.8	5.3	16.75	1.87	0.97
NGC2679 ^a	3.8	3.5	30.62	3.42	1.78
NGC2695	5.1	7.0	23.23	2.59	1.35
NGC2699	2.5	3.5	23.23	2.59	1.35
NGC2974	5.1	7.0	24.32	2.71	1.42
NGC3377	3.8	5.3	10.67	1.19	0.62
NGC3379	2.5	3.5	10.67	1.19	0.62
NGC3384	5.1	7.0	10.67	1.19	0.62
NGC3414	1.3	1.8	20.14	2.25	1.17
NGC3608	3.8	3.5	15.56	1.74	0.91
NGC4261 ^a	2.5	3.5	31.62	3.53	1.84
NGC4262	2.5	3.5	16.29	1.82	0.95
NGC4270	2.5	1.8	16.29	1.82	0.95
NGC4365 ^a	3.8	3.5	17.95	2.00	1.04
NGC4374	2.5	3.5	16.29	1.82	0.95
NGC4382	3.8	5.3	16.29	1.82	0.95
NGC4387	3.8	3.5	16.29	1.82	0.95
NGC4458	3.8	5.3	16.29	1.82	0.95
NGC4473	2.5	1.8	16.29	1.82	0.95
NGC4486	2.5	1.8	16.29	1.82	0.95
NGC4546	2.5	3.5	16.29	1.82	0.95
NGC4552	3.8	3.5	16.29	1.82	0.95
NGC4570	5.1	5.3	16.29	1.82	0.95
NGC5198	2.5	1.8	36.31	4.05	2.11
NGC5308	3.8	7.0	28.31	3.16	1.65
NGC5813	2.5	5.3	26.30	2.93	1.53
NGC5831	5.1	5.3	22.80	2.54	1.33
NGC5838	3.8	5.3	18.71	2.09	1.09
NGC5845	2.5	1.8	21.78	2.43	1.27
NGC5846	5.1	5.3	24.89	2.78	1.45
NGC5982	1.3	1.8	41.88	4.76	2.44
NGC6548 ^a	3.8	10.5	33.57	3.75	1.95

Columns: (1) Source name; (2)-(3) upper limits (1σ) in main beam temperature for the CO(1-0) and CO(2-1) lines; (4) adopted distance; (5)-(6) diameters of the CO(1-0) and CO(2-1) beams, in kpc.

Notes: a) galaxies observed by SAURON but not part of the representative sample of 48 E/S0s (see de Zeeuw et al. 2002).

suggestive that the metallicity-driven increase in CO luminosity per unit H_2 mass is more than compensated by the associated decrease in gas content.

The $L_{\text{FIR}}/M_{\text{H}_2}$ ratio is usually called the star formation efficiency (SFE), and somewhat surprisingly, the SAURON galaxies tend to have SFEs in the range of the highest values for normal spirals. The low average dust temperatures derived above are expected for such low values of the molecular gas content.

Figure 3 shows the so-called “Kennicutt-Schmidt diagram” (e.g. Kennicutt 1998) of our objects. This relates the star formation rate (SFR) surface density (as derived from the FIR luminosity and normalised by the area within R_{25} , the radius at the 25 mag arcsec^{-2} isophote in B) to the surface density of H_2 (the H_2 mass detected normalised by the same area). The normal spiral galaxy sample of Kennicutt (1998) is also plotted for comparison. Our sample objects

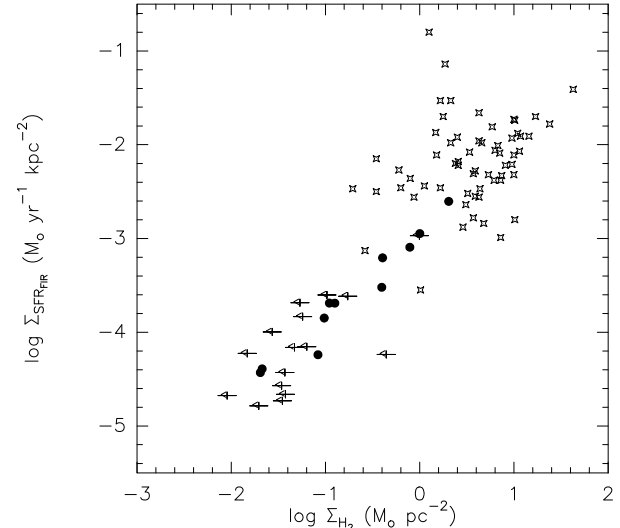


Figure 3. Kennicutt-Schmidt diagram of our sample galaxies, showing the FIR-derived star formation rate surface density as a function of the surface density of H_2 (see text). CO detections are shown with solid dots and upper limits by arrows. The normal spiral galaxy sample of Kennicutt (1998) is also plotted for comparison (stars).

appear to follow the same correlation as normal spirals, but the relation is tighter (at least for the detections) and extends that for normal spirals by almost 2 orders of magnitude down in SFR.

4 MOLECULAR MASS CORRELATIONS

We have explored many possible correlations of the molecular gas mass with other galaxy parameters available in catalogues or the literature, particularly the SAURON survey papers. Most quantities do not correlate significantly with H_2 mass, but a few do show interesting trends and are discussed below for the SAURON representative sample. Table 3 lists all the parameters used in those correlations.

No correlation was found between M_{H_2}/L_B and the galaxy inclination, the V/σ parameter quantifying rotational support or with any apparent flattening or axis ratio measured at any radius. Normally, face-on galaxies are much easier to detect in CO since they have very narrow line widths (all the emission is concentrated in a few channels), and conversely edge-on galaxies are harder to detect because of their broad line widths (the emission is spread out over many channels with low intensity) and possible confusion with a baseline ripple. However, the absence of a correlation between gas content and any inclination indicator in the present study suggests that there is no detection bias related to the line width.

4.1 Correlations with dust content

As a reference, we show in Figure 4 the relationship between molecular gas mass and $IRAS$ 60 μm luminosity, by far the strongest correlation we observe (see also the bottom-left panel in Fig. 2). All galaxies detected in CO are in fact also

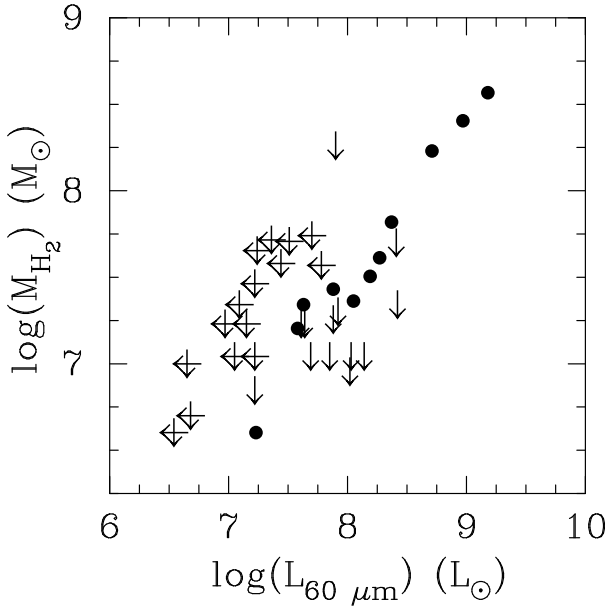


Figure 4. Molecular gas mass versus *IRAS* 60 μm luminosity for the **SAURON** representative sample. The correlation is excellent. Detections are shown with solid dots and upper limits by arrows.

detected by *IRAS*. They follow a very tight relation which, as suggested above, extends to lower H_2 masses a similar correlation for later galaxy types (e.g. Young & Scoville 1991).

As might be expected, the **SAURON** galaxies which are detected in CO also show dust features in the unsharp-masked optical images of Sarzi et al. (2006). The one exception to this statement is NGC7457, for which Welch & Sage (2003) report a small amount of molecular gas and which shows no small-scale dust feature beyond the nucleus ($R \gtrsim 1''$). The dust morphologies across the sample range from well developed large disks ($\gtrsim 10''$ diameter; e.g. NGC2685, NGC3032, NGC4459 and NGC4526) to small nuclear features ($\lesssim 5''$; e.g. NGC3156, NGC4150 and NGC4477) and even larger scale irregular patches or lanes (e.g. NGC3156, NGC4150, NGC3489 and NGC4278).

Dust morphologies are commonly assumed to indicate, at least qualitatively, how long the cold gas has been present in a galaxy, since it should take several dynamical times for the gas to settle into the most regular disks (e.g. Tran et al. 2001). If this argument holds for the molecular gas, we can infer that the galaxies with large, regular dust disks have had their cold gas longer than the galaxies with irregular dust morphologies (see also Sarzi et al. 2006). Interferometric maps revealing the kinematics of the molecular gas should give more quantitative insights into its origin.

4.2 Correlations with structural parameters

Even within the narrow morphological range defined by the E/S0s of the **SAURON** representative sample, Figure 5 shows that earlier type galaxies (which are also generally more luminous and massive) have relatively less molecular gas per unit luminosity than later type galaxies. It is also clear that our detections are almost exclusively confined to the later types, in agreement with the standard view of early-type galaxies being gas poor with little to no star forma-

tion. Those trends are consistent with previous results (e.g. Lees et al. 1991; Sage et al. 2006) but are not very strong, which could be due to the compensating effects of metallicity and evolution mentioned above.

4.3 Correlations with stellar populations

Figure 6 shows the absorption line-strength indices of $\text{H}\beta$, Fe5015 and Mgb , measured within one effective radius R_e (the radius encompassing half the light) with **SAURON** (see Kuntschner et al. 2006), as a function of the molecular gas content normalised by the blue luminosity. There is a clear trend in the sense that the galaxies with large $\text{H}\beta$ line-strengths are more likely to have detectable CO emission. Galaxies with smaller Fe5015 and Mgb indices are also more likely to be detected. Similar results are obtained when the optical indices are measured within a smaller aperture ($R_e/8$).

$\text{H}\beta$ is primarily a tracer of age, especially at high values ($\text{H}\beta \gtrsim 2.0$), suggesting that galaxies with younger stellar populations are relatively richer in molecular gas. This is of course expected since stars are born within molecular clouds, but to our knowledge this correlation is observed here for the first time. The Fe5015 and Mgb indices can respectively be thought of as tracing the metallicity and α -element abundance, which could suggest that CO-rich galaxies are more metal and α -element poor (and thus may have had a slow star formation fuelled by relatively pristine gas), but those relationships and inferences are less straightforward. More direct probes of the star formation and stellar population parameters are thus preferable.

4.4 Correlations with star formation

Figure 7 shows correlations of the molecular gas content (normalised by the blue luminosity) with three star formation indicators, namely the $\text{H}\alpha$ luminosity within the **SAURON** field-of-view (Sarzi et al. 2006), the effective $B - V$ colour and the age of the stellar populations, the latter derived from line-strength indices measured in a $4'' \times 4''$ central aperture assuming a single stellar population (McDermid et al. 2006). No clear correlation is seen, except perhaps with colour, but it is clear that CO-rich galaxies have preferentially large $\text{H}\alpha$ luminosities, blue colours, and young ages. In fact, all the galaxies detected in CO and with a measured age have a central luminosity-weighted stellar ages less than 3.5 Gyr. No clear trend is seen with the derived metallicity or α -element abundance (McDermid et al. 2006; not shown), strongly suggesting that the trends with line-strength indices discussed above are in fact primarily or perhaps exclusively driven by age, with little dependence on the metallicity or α -element abundance.

4.5 Correlations with stellar kinematics

It is interesting to enquire about possible correlations between the CO content of the **SAURON** sample galaxies and their stellar dynamics. Using the stellar kinematic maps of Emsellem et al. (2004) and McDermid et al. (2006), it is relatively easy to identify discrete kinematic structures such as central stellar discs and KDCs. In fact, McDermid et al.

Table 3. Galaxy parameters for the SAURON representative sample.

Galaxy	M_{H_2} ($10^8 M_{\odot}$)	Type	M_B (mag)	σ_c (km s $^{-1}$)	$L_{60\mu\text{m}}$ (L_{\odot})	$L_{\text{H}\alpha}$ (erg s $^{-1}$)	$(B - V)_e$ (mag)	$\text{H}\beta$ (Å)	Fe5015 (Å)	Mgb (Å)	Age_c (Gyr)	i (deg)	V/σ
(1)	(2)	(3)	(4)	(5)	(6)	(7)	(8)	(9)	(10)	(11)	(12)	(13)	(14)
NGC 474	< 0.38	-2.2	-20.42	170	<7.44	39.44	0.940	1.81	4.85	3.45	—	42	—
NGC 524	—	-1.5	-21.40	245	8.92	39.00	1.070	1.50	5.38	4.20	—	9	—
NGC 821	—	-4.2	-20.44	208	<7.35	—	1.020	1.57	4.65	3.72	—	69	0.4
NGC1023	< 0.04	-2.6	-20.42	206	<6.54	38.46	1.010	1.51	4.98	4.19	4.7	90	1.1
NGC2549	< 0.18	-2.0	-19.36	146	7.88	38.80	0.955	2.02	5.10	3.54	2.5	90	1.0
NGC2685	0.27	-0.7	-19.05	99	7.88	39.37	0.935	2.04	4.21	3.04	—	72	1.1
NGC2695	< 0.45	-2.4	-19.38	220	<7.24	—	0.980	1.27	4.34	3.94	10.2	52	0.8
NGC2699	< 0.23	-5.0	-18.85	—	—	38.02	0.980	1.76	4.76	3.58	1.5	29	—
NGC2768	0.41	-3.1	-21.15	188	8.27	39.65	0.960	1.64	4.43	3.64	2.5	75	0.8
NGC2974	< 0.50	-3.6	-20.32	229	8.41	39.96	1.005	1.71	5.14	4.09	7.9	75	0.9
NGC3032	2.54	-1.7	-18.77	82	8.97	39.42	0.630	3.98	4.02	2.14	0.9	31	—
NGC3156	0.22	-2.4	-18.08	84	7.63	39.18	0.770	3.00	3.66	1.79	—	66	0.9
NGC3377	< 0.07	-4.1	-19.24	136	7.22	38.96	0.905	1.86	4.37	3.20	—	90	0.7
NGC3379	< 0.05	-4.1	-20.16	206	<6.68	38.18	0.975	1.44	4.81	4.15	11.5	30	0.2
NGC3384	< 0.10	-2.6	-19.56	142	<6.65	37.92	0.955	1.84	5.12	3.70	3.2	90	0.9
NGC3414	< 0.09	-2.5	-19.78	246	8.02	39.72	0.930	1.50	4.49	3.72	3.6	40	0.9
NGC3489	0.12	-2.1	-19.32	138	—	39.64	0.845	2.60	4.40	2.60	1.7	63	0.5
NGC3608	< 0.15	-4.3	-19.54	204	—	38.15	1.000	1.60	4.73	3.75	8.9	51	0.1
NGC4150	0.66	-2.4	-18.48	148	8.37	38.91	0.830	2.87	4.11	2.35	1.5	55	—
NGC4262	< 0.11	-2.6	-18.88	186	7.69	39.41	0.970	1.49	4.46	3.90	10.2	30	—
NGC4270	< 0.11	-1.1	-18.28	140	<7.05	—	0.950	1.74	4.67	3.24	—	78	0.7
NGC4278	0.23	-4.6	-19.93	252	8.05	39.95	0.960	1.41	4.59	4.21	—	27	0.2
NGC4374	< 0.11	-3.5	-21.23	297	8.14	39.30	1.000	1.42	4.66	4.08	—	35	0.1
NGC4382	< 0.17	-1.8	-21.28	177	7.61	—	0.895	1.98	4.72	3.36	1.7	45	0.4
NGC4387	< 0.17	-3.4	-18.34	117	<7.15	—	0.965	1.51	4.42	3.67	—	66	0.5
NGC4458	< 0.17	-3.8	-18.42	102	<6.97	—	0.915	1.59	3.97	3.27	—	25	0.2
NGC4459	1.70	-2.0	-19.99	174	8.71	38.89	0.970	1.85	4.68	3.43	1.9	46	0.4
NGC4473	< 0.11	-4.2	-20.26	191	<7.22	—	0.990	1.50	4.88	4.03	13.2	90	0.3
NGC4477	0.32	-1.8	-19.96	172	8.19	39.42	0.970	1.59	4.71	3.84	—	28	0.2
NGC4486	< 0.11	-4.0	-21.79	351	8.03	39.70	0.980	1.15	4.70	4.62	15.1	65	0.0
NGC4526	3.69	-1.6	-20.68	256	9.18	39.22	0.975	1.62	4.93	4.16	2.8	90	1.0
NGC4546	< 0.11	-2.6	-19.98	242	7.85	39.74	0.990	1.54	4.64	3.92	—	90	0.9
NGC4550	0.16	-2.3	-18.83	80	7.58	39.29	0.890	1.99	4.32	2.93	—	90	1.5
NGC4552	< 0.17	-3.3	-20.58	264	7.64	38.69	1.000	1.37	5.33	4.55	8.9	29	0.0
NGC4564	—	-4.1	-19.39	168	—	—	0.965	1.55	4.85	4.00	3.6	90	0.9
NGC4570	< 0.22	-1.7	-19.54	188	<7.09	36.94	0.970	1.45	4.79	3.99	—	90	—
NGC4621	—	-4.0	-20.64	245	<7.05	—	0.975	1.43	4.75	4.14	6.9	54	0.5
NGC4660	—	-4.1	-19.22	191	<7.13	—	0.990	1.47	4.80	4.07	—	50	0.8
NGC5198	< 0.55	-3.4	-20.38	195	<7.70	39.13	0.985	1.56	4.70	3.93	15.1	38	0.0
NGC5308	< 0.51	-1.1	-20.27	260	<7.51	—	0.925	1.46	4.92	4.23	—	90	0.9
NGC5813	< 0.29	-4.5	-20.99	238	<7.22	39.36	1.010	1.52	4.74	4.12	15.1	57	0.0
NGC5831	< 0.44	-4.2	-19.73	175	—	38.19	0.985	1.78	4.78	3.32	3.2	39	0.2
NGC5838	< 0.22	-3.0	-19.87	274	8.42	38.79	1.010	1.58	5.05	4.19	—	90	0.8
NGC5845	< 0.20	-4.1	-18.58	221	7.92	—	1.120	1.52	5.38	4.41	8.9	69	0.6
NGC5846	< 0.52	-4.2	-21.24	250	<7.36	39.48	1.030	1.32	4.89	4.38	7.9	25	0.0
NGC5982	< 0.37	-3.9	-21.46	251	<7.78	38.99	0.940	1.60	5.18	3.98	13.2	62	0.3
NGC7332	< 1.82	-1.7	-19.93	134	7.90	39.67	0.905	2.16	4.80	3.17	—	90	1.0
NGC7457	0.04	-2.2	-18.81	75	7.23	38.23	0.900	2.25	4.33	2.68	—	67	1.0

Columns: (1) NGC number; (2) CO-derived H₂ mass (this paper); (3) Morphological type (HyperLEDA: <http://leda.univ-lyon1.fr/>; de Zeeuw et al. 2002); (4) Total absolute blue magnitude (de Zeeuw et al. 2002); (5) Central stellar velocity dispersion (HyperLEDA; de Zeeuw et al. 2002); (6) *IRAS* 60 μm luminosity (logarithmic; NED: <http://nedwww.ipac.caltech.edu/index.html>); (7) Total H α luminosity within the SAURON field-of-view, derived assuming an H α /H β flux ratio of 2.86 (logarithmic; Sarzi et al. 2006); (8) Effective $B - V$ color (HyperLEDA; de Zeeuw et al. 2002); (9)–(11) Absorption line-strength indices, luminosity-weighted over an effective radius (Kuntschner et al. 2006); (12) luminosity-weighted age of the stellar populations, as derived from line-strength indices measured in a central 4'' × 4'' aperture assuming a single stellar population (McDermid et al. 2006); (13) Inclination (HyperLEDA); (14) Rotational support diagnostic V_{rot}/σ (HyperLEDA).

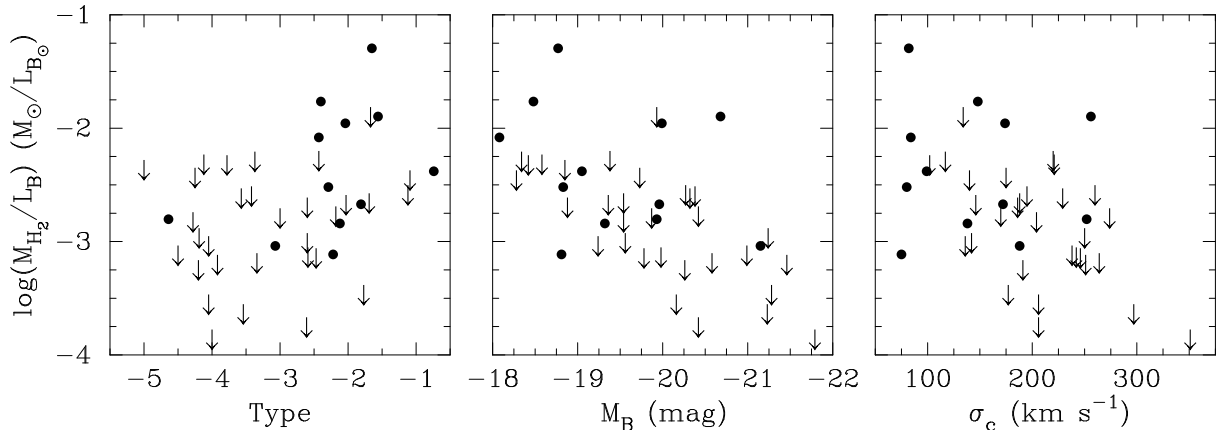


Figure 5. Molecular gas content (normalised by the total blue luminosity) versus structural parameters for the SAURON representative sample. **Left:** Morphological type (HyperLEDA; de Zeeuw et al. 2002). **Centre:** Total absolute B magnitude (de Zeeuw et al. 2002). **Right:** Central stellar velocity dispersion (HyperLEDA). Detections are shown with solid dots and upper limits by arrows.

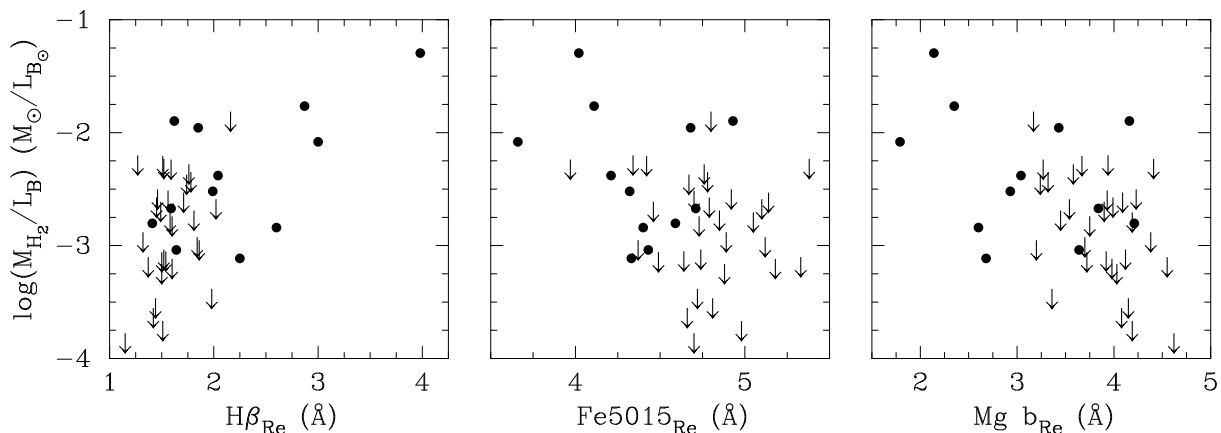


Figure 6. Molecular gas content (normalised by the total blue luminosity) versus absorption line-strength indices (luminosity-weighted within one effective radius) from Kuntschner et al. (2006) for the SAURON representative sample. **Left:** $H\beta$ index. **Centre:** $Fe5015$ index. **Right:** Mgb index. Detections are shown with solid dots and upper limits by arrows.

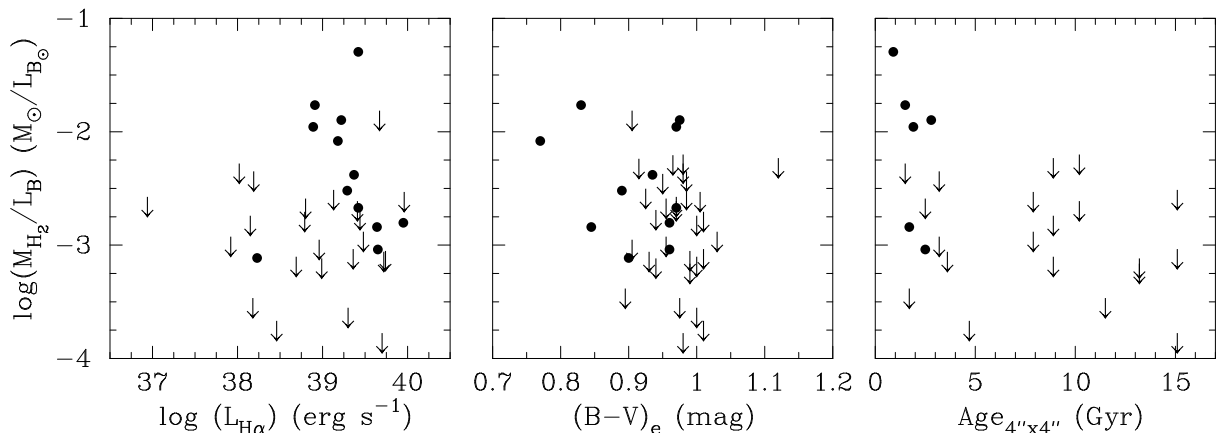


Figure 7. Molecular gas content (normalised by the total blue luminosity) versus various star formation indicators for the SAURON representative sample. **Left:** $H\alpha$ luminosity within the SAURON field-of-view, derived assuming an $H\alpha/H\beta$ flux ratio of 2.86 (Sarzi et al. 2006). **Centre:** Effective $B - V$ colour (HyperLEDA; de Zeeuw et al. 2002). **Right:** Luminosity-weighted stellar age, derived from line-strength indices measured in a $4'' \times 4''$ central aperture assuming a single stellar population (McDermid et al. 2006). Detections are shown with solid dots and upper limits by arrows.

(2006) identified two classes of KDCs among the **SAURON** galaxies. One class is made up of compact KDCs with diameters $\lesssim 300$ pc, which are often (though not exclusively) young, and the other class consists of homogeneously old and extended kpc-scale KDCs. Interestingly, half of the compact KDCs are detected in CO (NGC3032, NGC4150 and NGC7457; the three youngest ones), but none of the large KDCs are. While some of the KDCs may well have formed through dissipationless processes, the presence of molecular gas in the young, compact KDCs convincingly argues that at least some of the KDCs form through dissipative processes in which gas sinks to the center of the galaxy and forms stars.

In addition to the compact KDCs, there are other cases which show probable associations between the molecular gas and stellar kinematic substructures. For example, NGC 4526 is the most CO-rich galaxy in the **SAURON** sample, and it has a large dynamically cold stellar disk (Emsellem et al. 2004) which shows young stellar ages in its H β absorption line strengths (Kuntschner et al. 2006). The properties of NGC 4459 are similar though not as extreme. These cases are analogous to the compact, young KDCs in that the molecular gas can probably be linked to the growth of a kinematically decoupled stellar component.

Surprisingly, however, in a broader comparison of molecular gas content to all types of kinematic substructure, we find that there is no strong correlation between the existence of a decoupled kinematic component and the presence of molecular gas. The fraction of galaxies with (or without) apparent kinematic substructure in the maps of Emsellem et al. (2004) is the same among CO detections and non-detections (and among the entire **SAURON** sample). Conversely, the CO detection (or non-detection) rate is the same among galaxies with and without stellar kinematic substructure (and again among the entire **SAURON** sample). The sample thus contains some galaxies with kinematic substructure and no detectable molecular gas, as well as some galaxies with molecular gas and no detectable kinematic substructure.

These facts do not lend themselves to a simple, straightforward picture of the relationships between molecular gas and kinematic substructure. In some cases there may be a direct link as a new stellar substructure grows out of the molecular gas; in other cases the stellar kinematic substructures may be relics of past events completely unrelated to the current molecular gas content. Synthesis observations of our detections should shed new light on those questions, allowing direct comparisons of the distribution and kinematics of CO, stars, and ionised gas at similar spatial resolutions.

4.6 Aperture correction

As mentioned above, the 30 m beam at both CO(1-0) and CO(2-1) only covers a small fraction of the optical extent of the galaxies. Although the results of Young (2002, 2005) suggest that our beams should recover all the CO in typical nearby early-type galaxies, the same could in principle also be true of the molecular gas extent, and one should correct the CO fluxes to a fixed physical aperture for all galaxies in the sample. That aperture should preferentially be related to the molecular gas extent, but failing this (since we do

not know the typical CO distribution), to a characteristic optical radius.

We have thus attempted to correct our fluxes assuming a uniform molecular gas surface density within one optical effective radius R_e , within the optical radius R_{25} , or assuming an exponential distribution of effective radius equal to that in the optical. Such corrections were often large and only give the general impression of adding even more scatter to the plots we have shown. This suggests that the molecular gas does not have a characteristic spatial extent and is not strongly correlated to the stellar extent.

5 FAR-INFRARED-RADIO CORRELATION

As illustrated above, galaxies which contain substantial amounts of molecular gas are likely to have some star formation activity. As a further attempt to understand the star formation properties of the **SAURON** early-type galaxies, we turn to an analysis of their FIR and radio continuum emission. It has been known for some time that if one defines a logarithmic FIR to radio continuum flux ratio as

$$q \equiv \log\left(\frac{FIR}{3.75 \times 10^{12} \text{ W m}^{-2}}\right) - \log\left(\frac{S_{1.4\text{GHz}}}{\text{W m}^{-2} \text{ Hz}^{-1}}\right), \quad (2)$$

then the bulk of the gas-rich, star forming galaxies lie in a tight band at $q \approx 2.34$, with a dispersion of about 0.26 dex (Condon 1992; Yun, Reddy & Condon 2001). The small dispersion in q values is normally interpreted to mean that both the FIR emission and the cm-wave radio continuum emission are powered by star formation activity. Galaxies whose cm-wave radio continuum emission is dominated by an active galactic nucleus (AGN) are usually easy to identify by their low q values.

There is good evidence that the radio continuum emission of early type galaxies arises from both star formation and AGN activity, different processes dominating in different galaxies. From an early analysis of the NVSS data (e.g. Condon et al. 1998), Cotton & Condon (1998) found that one quarter of the E and S0 galaxies detected by NVSS and *IRAS* “have IR/radio flux density ratios suggestive of star formation,” whereas the other three quarters are probably powered by AGN. Wrobel & Heeschen (1988) obtained high resolution radio images and showed that six early-type galaxies which lie on the FIR-radio correlation indeed have extended kpc-scale radio morphologies, consistent with star formation rather nuclear activity.

If the early-type galaxies which lie on the FIR-radio correlation are indeed experiencing star formation, and the star formation has an efficiency typical of that in spirals, we should expect to find that the early-type galaxies on the FIR-radio correlation are also the ones with molecular gas. In short, a comparison of q values and CO content in early-type galaxies should reveal something about the nature of star formation and the fate of the molecular gas in those objects.

Figures 8–9 and Table 4 show FIR and radio continuum fluxes, luminosities and q values for the sample galaxies. *IRAS* fluxes are taken from the NASA Extra-

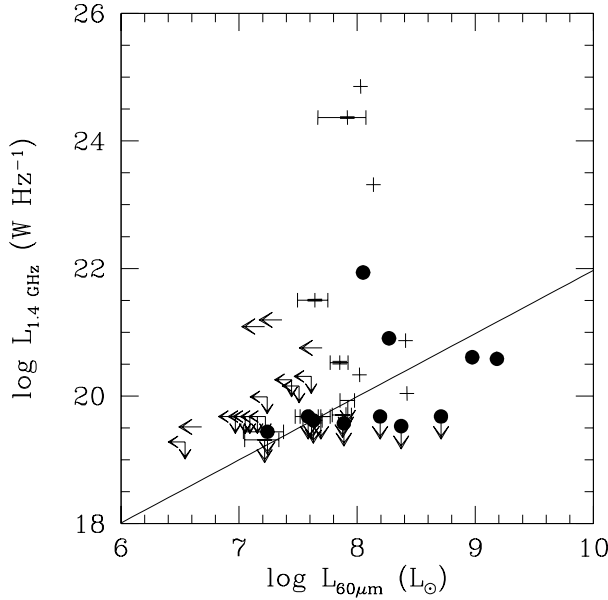


Figure 8. 1.4 GHz radio luminosities versus *IRAS* 60 μ m luminosities. CO detections are indicated with filled circles and upper limits by arrows. Error bars (1σ) are shown only if they are larger than the symbol size. The solid line shows the fit $\log(L_{1.4\text{GHz}}) = 0.99 \log(L_{60\mu\text{m}}/L_\odot) + 12.07$ which Yun et al. (2001) obtained for a sample of 1809 galaxies of all types with $S_{60\mu\text{m}} > 2$ Jy. Distance uncertainties are not incorporated into the error bars.

galactic Database¹ (NED). The 1.4 GHz fluxes were obtained from the NVSS catalogue (Condon et al. 1998) with three exceptions: NGC4261, NGC4374 and NGC4486 are highly resolved by NVSS so their fluxes are taken from White & Becker (1992). Galaxies that are not detected in the NVSS are assigned a 3σ upper limit of 1.5 mJy. Of the 47 galaxies with CO data, we are able to calculate a q value or limit for 32 (68%). The remaining 15 are undetected at all three wavelengths or were not observed by *IRAS*.

The SAURON sample of early-type galaxies spans the full range of FIR and radio properties. Following Yun et al. (2001), we define “radio-excess” and “IR-excess” galaxies to have q values respectively higher and lower than the average by 0.7 dex ($\approx 2.7\sigma$). Of the 32 galaxies for which we have both CO data and a q value, 9 galaxies² fall in the radio-excess category. Their radio continuum emission is most likely dominated by AGN activity (Reddy & Yun 2004). Two galaxies fall in the IR-excess category³, which is more poorly understood. As discussed more fully by Yun et al. (2001), an IR excess may indicate unusually warm dust from a compact starburst or a dust-enshrouded AGN. Alternatively, an IR excess could suggest that the galaxy has a smaller-than-usual synchrotron output due to a weak interstellar magnetic field. Such IR excesses are rare, however, only accounting for 9 of 1809 IR-selected galaxies in the sample of Yun et al. (2001). In our sample, 21 galaxies having

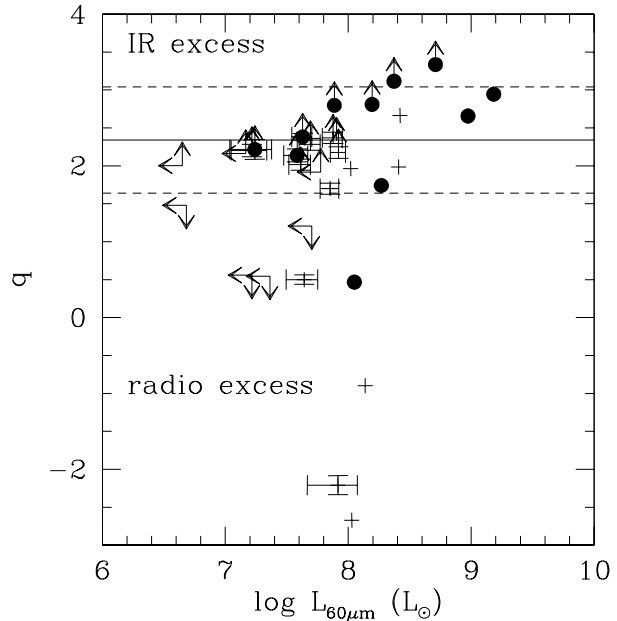


Figure 9. *IRAS* FIR/radio continuum flux ratio q (see text) versus 60 μ m luminosities. The solid line marks the average value $q = 2.34$ derived by Yun et al. (2001). The dotted lines delineate the “radio-excess” and “IR-excess” regions defined by Yun et al. (2001) as having FIR/radio flux ratios 5 times larger or smaller than the mean. For a dispersion of 0.26 dex, these lines lie $\approx 2.7\sigma$ away from the mean. As in Figure 8, CO detections are indicated with filled circles, upper limits by arrows, and error bars are shown only if they are larger than the symbol sizes.

both CO data and a q value lie within the “average” band of $q = 2.34 \pm 0.7$, although 14 of those only have upper limits for their radio continuum flux, and could conceivably move into the IR-excess category if their radio continuum fluxes are a good deal smaller than the current 1.5 mJy limit.

The CO detection rate is significantly lower among the radio-excess galaxies (1/9 or 11%) than among the “average” and IR-excess galaxies (10/23 or 43%) (both IR-excess galaxies are detected). Thus, early-type galaxies with $q \gtrsim 2.3$ are more likely to also contain molecular gas, the raw material for star formation. This association between molecular gas and $q \gtrsim 2.3$ bolsters the contention of Wrobel & Heeschen (1988) that early-type galaxies with a q value similar to that of spirals are also experiencing star formation.

If it is true that early-type galaxies with $q \gtrsim 2.3$ have FIR and radio emissions which are primarily powered by star formation, then 23 of the 32 SAURON early-type galaxies with CO data and estimated q values show evidence for star formation activity. Curiously, however, several galaxies which are not detected in CO emission also have $q \approx 2.3$. Especially notable are NGC2974, NGC3414, NGC4546 and NGC5838, which have FIR and radio fluxes within the ranges occupied by galaxies detected in CO (e.g. Fig. 8). On the other hand, NGC2974 does show evidence for recent star formation in the ultraviolet (Jeong et al. 2007), and all four galaxies have substantial amounts of ionised gas (e.g. Sarzi et al. 2006). If $q \approx 2.3$ really is an indicator of star formation activity, then perhaps these galaxies have abundant molecular gas but low CO/H₂ ratios, or alternatively they could have

¹ <http://nedwww.ipac.caltech.edu/index.html>

² NGC3379, NGC4261, NGC4278, NGC4374, NGC4486, NGC4552, NGC5198, NGC5813 and NGC5846 are radio-excess galaxies.

³ NGC4150 and NGC4459 are IR-excess galaxies.

Table 4. FIR and radio parameters of the sample galaxies.

Galaxy (1)	D (Mpc) (2)	$S_{100\mu\text{m}}$ (Jy) (3)	$S_{60\mu\text{m}}$ (Jy) (4)	$P_{20\text{cm}}$ (mJy) (5)	q (6)
NGC 474	31.62	< 0.10	< 0.027	< 1.5	—
NGC 524	32.81	2.05 (0.13)	0.76 (0.03)	3.1 (0.4)	2.64 (0.06)
NGC 821	23.55	0.50 (0.12)	< 0.041	< 1.5	> 2.13
NGC1023	10.28	< 0.075	< 0.032	< 1.5	—
NGC2549	16.75	0.37 (0.13)	0.26 (0.05)	< 1.5	> 2.37
NGC2679 ^a	30.62	—	—	< 1.5	—
NGC2685	14.39	1.87 (0.11)	0.36 (0.04)	< 1.5	> 2.80
NGC2695	23.23	< 0.11	< 0.031	< 1.5	—
NGC2699	23.23	—	—	< 1.5	—
NGC2768	21.48	1.37 (0.06)	0.39 (0.03)	14.5 (0.6)	1.74 (0.03)
NGC2974	24.32	1.90 (0.05)	0.42 (0.03)	10.4 (0.5)	1.98 (0.03)
NGC3032	21.68	4.7 (0.09)	1.94 (0.03)	7.2 (0.5)	2.66 (0.03)
NGC3156	15.14	0.61 (0.08)	0.18 (0.03)	< 1.5	> 2.38
NGC3377	10.67	0.35 (0.07)	0.14 (0.05)	< 1.5	> 2.20
NGC3379	10.67	< 0.11	< 0.041	2.4 (0.5)	< 1.48
NGC3384	10.67	0.45 (0.09)	< 0.038	< 1.5	> 2.00
NGC3414	20.14	0.56 (0.19)	0.25 (0.03)	4.4 (0.4)	1.96 (0.08)
NGC3489	10.67	—	—	< 1.5	—
NGC3608	15.56	—	—	< 1.5	—
NGC4150	13.68	2.67 (0.06)	1.22 (0.04)	< 1.5	> 3.12
NGC4261 ^a	31.62	0.15 (0.05)	0.08 (0.04)	$19 (0.6) \times 10^3$	-2.21 (0.13)
NGC4262	16.29	0.39 (0.12)	0.18 (0.04)	< 1.5	> 2.28
NGC4270	16.29	< 0.094	< 0.041	< 1.5	—
NGC4278	13.68	1.86 (0.06)	0.58 (0.05)	385 (12)	0.47 (0.02)
NGC4365 ^a	17.95	0.65 (0.13)	< 0.044	< 1.5	> 2.16
NGC4374	16.29	1.16 (0.12)	0.5 (0.03)	$6.5 (0.2) \times 10^3$	-0.90 (0.03)
NGC4382	16.29	< 0.076	0.15 (0.03)	< 1.5	> 1.94
NGC4387	16.29	< 0.178	< 0.052	< 1.5	—
NGC4458	16.29	< 0.142	< 0.034	< 1.5	—
NGC4459	16.29	4.82 (0.13)	1.87 (0.07)	< 1.5	> 3.34
NGC4473	16.29	< 0.107	< 0.061	< 1.5	—
NGC4477	16.29	1.41 (0.10)	0.57 (0.05)	< 1.5	> 2.81
NGC4486	16.29	0.41 (0.10)	0.39 (0.04)	$224 (6.7) \times 10^3$	-2.67 (0.047)
NGC4526	16.29	17.1 (0.09)	5.56 (0.05)	12 (0.5)	2.94 (0.02)
NGC4546	16.29	0.89 (0.22)	0.26 (0.05)	10.5 (0.5)	1.70 (0.07)
NGC4550	16.29	0.25 (0.09)	0.14 (0.03)	< 1.5	> 2.14
NGC4552	16.29	0.53 (0.06)	0.16 (0.05)	100 (3)	0.50 (0.06)
NGC4564	16.29	< 0.19	< 0.060	< 1.5	—
NGC4570	16.29	< 0.11	< 0.045	< 1.5	—
NGC4621	16.29	< 0.094	< 0.050	< 1.5	—
NGC4660	16.29	< 0.10	< 0.048	< 1.5	—
NGC5198	36.31	< 0.077	< 0.037	3.6 (0.4)	< 1.21
NGC5308	28.31	< 0.089	< 0.039	< 1.5	—
NGC5813	26.30	< 0.10	< 0.023	14.8 (1)	< 0.56
NGC5831	22.80	—	—	< 1.5	—
NGC5838	18.71	1.67 (0.09)	0.73 (0.04)	2.6 (0.4)	2.66 (0.07)
NGC5845	21.78	0.23 (0.10)	0.17 (0.02)	< 1.5	> 2.18
NGC5846	24.89	< 0.127	< 0.036	21 (1.3)	< 0.55
NGC5982	41.88	0.37 (0.04)	< 0.033	< 1.5	> 1.92
NGC6548 ^a	33.57	< 0.119	< 0.035	< 1.5	—
NGC7332	19.23	0.41 (0.11)	0.21 (0.03)	< 1.5	> 2.33
NGC7457	12.36	0.45 (0.19)	0.11 (0.04)	< 1.5	> 2.22

Columns: (1) Source name; (2) adopted distance; (3)–(4) 100 and 60 μm fluxes (NED); (5) 20 cm radio continuum power (Condon et al. 1998; White & Becker 1992); (6) FIR/radio continuum flux ratio. Uncertainties are quoted in parentheses.

Notes: a: galaxies observed by **SAURON** but not part of the representative sample of 48 E/S0s.

smaller molecular gas contents but more efficient star formation. There might even also be some other processes beside star formation which produce their FIR and radio fluxes.

The entire sample having CO data contains 22 galaxies traditionally classified as elliptical and 25 lenticulars. As discussed in Section 3.2, CO is detected in only 2 ellipticals but in 10 lenticulars, a much higher detection rate. In contrast, the ellipticals show more AGN activity. Of all galaxies for which we could calculate q (see Table 4), 9 of 17 ellipticals show a radio excess but none of the 17 S0s does. We caution however that detailed studies of the morphology and kinematics of the SAURON early-type galaxies (e.g. Emsellem et al. 2004; Sarzi et al. 2006) prompt some reclasifications.

6 CONCLUSIONS

We surveyed in the CO(1-0) and CO(2-1) lines early-type galaxies observed in the optical with the SAURON integral-field spectrograph. Taking into account literature results, the detection rate for the SAURON representative sample of 48 E/S0s is 12/43 or 28%. This is lower than previous surveys but differences can probably be explained by differences between the samples. Our data extend the usual correlations between FIR luminosity, dust mass and molecular mass of later galaxy types, as well as the related correlation between star formation and molecular gas surface density. Unsurprisingly, the more massive and luminous earlier type galaxies have a relatively lower molecular gas content and the local galaxy density does not appear to have a strong effect on the molecular content.

Although weak, indicative trends are nevertheless observed with various optical absorption line-strength indices. CO-rich galaxies tend to have higher H β and lower Fe5015 and Mgb indices. CO-rich galaxies also show the strongest evidence of star formation, probed in a variety of ways, suggesting that those trends are primarily driven by stellar age. Analysing the FIR and radio fluxes, we similarly see that so-called “radio-excess” galaxies, presumably powered by active galactic nuclei, are significantly poorer in molecular gas than so-called “IR-excess” galaxies, presumably powered by star formation. These trends support the recent *Galaxy Evolution Explorer* (GALEX) ultraviolet results (among others), which suggest that a significant number of early-type galaxies may be undergoing a small amount of star formation activity (e.g. Yi et al. 2005). Here, however, we have apparently found the raw material for this residual star formation, and have demonstrated that it is actively being transformed. This might not be surprising in spiral galaxies, but it is a significant step for early-types.

Overall, however, the weakness of the correlations between the CO content and most optically-derived parameters suggests that, in many of these galaxies, the molecular gas does not come from internal sources such as stellar mass loss. Instead the gas has probably been accreted and has properties largely independent from the old stellar component.

The current CO detections offer the possibility to pursue those issues with much improved spatially-resolved synthesis data, which can be directly compared to optical

integral-field observations at similar spatial resolution. Much work along those lines is already ongoing.

ACKNOWLEDGMENTS

The authors would like to thank the many people from the SAURON team, and in particular Eric Emsellem, for useful discussions. FC and LMY acknowledge support from the PPARC visitor grant PPA/V/S/2002/00553 to Oxford University during part of this work. LMY also thanks the Oxford Astrophysics Department for its hospitality during sabbatical work. This work is based on observations made with the IRAM 30 m telescope, in Pico Veleta, near Granada, Spain. This project made use of the HyperLEDA and NED databases.

REFERENCES

- Bacon R., et al., 2001, MNRAS, 326, 23
- Barnes J.E., 2002, MNRAS, 333, 481
- Bender R., 1988, A&A, 202, L5
- Bettoni D., Galletta G., Garcia-Burillo S., 2003, A&A, 405, 5
- Bournaud F., Jog C. J., Combes F., 2005, A&A, 437, 69
- Braine J., Combes F., 1992, A&A, 264, 433
- Bregman J. N., Hogg D. E., Roberts M. S., 1992, ApJ, 387, 484
- Casoli F., Boissé P., Combes F., Dupraz C., 1991, A&A, 249, 359
- Ciotti L., d’Ercole A., Pellegrini S., Renzini A., 1991, ApJ, 376, 380
- Combes F., Prugniel P., Rampazzo R., Sulentic J. W., 1994, A&A, 281, 725
- Condon J. J., 1992, ARA&A, 30, 575
- Condon J. J., Cotton W. D., Greisen E. W., Yin Q. F., Perley R. A., Taylor G. B., Broderick J. J., 1998, AJ, 115, 1693
- Cotton W. D., Condon J. J., 1998, in Bremer M. N., Jackson N., Perez-Fournon I., eds., Observational Cosmology with the New Radio Surveys. Kluwer, Dordrecht, p. 45
- Davies R. L., et al., 2001, ApJL, 548, L33
- de Zeeuw P.T., et al., 2002, MNRAS, 329, 513
- Emsellem E., et al., 2004, MNRAS, 352, 721
- Emsellem E., et al., 2006, MNRAS, submitted
- Faber S. M., et al., 1997, AJ, 114, 1771
- Ferrari F., Pastoriza M. G., Macchietto F., Caon N., 1999, A&AS, 136, 269
- Franx M., Illingworth G., Heckman T., 1989, ApJ, 344, 613
- Hibbard J. E., Guhathakurta P., van Gorkom J. H., Schweizer F., 1994, AJ, 107, 67
- Hildebrand R. H., 1983, QJRAS, 24, 267
- Hogg D. E., Roberts M. S., Sandage A., 1993, AJ, 106, 970
- Israel F. P., Tacconi L. J., Baas F., 1995, A&A, 295, 599
- Jeong H., Bureau M., Yi S. K., Krajnović D., Davies R. L., 2007, MNRAS, in press
- Kenney J. D. P., Young J. S., 1989, ApJ, 344, 171
- Kennicutt R. C. Jr., 1998, ApJ, 498, 541
- Knapp G. R., Rupen M. P., 1996, ApJ, 460, 271
- Kuntschner H., et al., 2006, MNRAS, 369, 497

Lees F., Knapp G. R., Rupen M. P., Phillips T. G., 1991, *ApJ*, 379, 177

Leon S., Combes F., Menon T. K., 1998, *A&A*, 330, 37

Leeuw L. L., Sansom A. E., Robson E. I., Haas M., Kuno N., 2004, *ApJ*, 612, 837

McDermid R. M., et al., 2006, *MNRAS*, 373, 906

Morganti R., et al., 2006, *MNRAS*, 371, 157

Naab T., Jesseit R., Burkert A., 2006, *MNRAS*, 372, 839

Nieto J.-L., Capaccioli M., Held E. V., 1988, *A&A*, 195, L1

Nieto J.-L., Bender R., Surma P., 1991, *A&A*, 244, L37

Reddy N. A., Yun M. S., 2004, *ApJ*, 600, 695

Sage L. J., Welch G. A., 2006, *ApJ*, 644, 850

Sage L. J., Welch G. A., Young L. M., 2006, *ApJ*, in press (astro-ph/0608179)

Sage L. J., Salzer J. J., Loose H.-H., Henkel C., 1992, *A&A*, 265, 19

Sage L. J., 1993, *A&A*, 272, 123

Sage L. J., Wrobel J. M., 1989, *ApJ*, 344, 204

Sanders D. B., Scoville N. Z., Soifer B. T., 1991, *ApJ*, 370, 158

Sanders D. B., Mirabel I. F., 1996, *ARA&A*, 34, 749

Sarzi M., et al., 2006, *MNRAS*, 366, 1151

Schinnerer E., Scoville N., 2002, *ApJ*, 577, L103

Scorza C., Bender R., Winkelmann C., Capaccioli M., Macchetto D. F., 1998, *A&AS*, 131, 265

Seifert W., Scorza C., 1996, *A&A*, 310, 75

Solomon P. M., Sage L. J., 1988, *ApJ*, 613, 334

Statler T. S., Emsellem E., Peletier R. F., Bacon R., 2004, *MNRAS*, 353, 1

Thronson H. A. Jr., Tacconi L., Kenney J., Greenhouse M. A., Margulis M., Tacconi-Garman L., Young J. S., 1989, *ApJ*, 344, 747

Tinney C. G., Scoville N. Z., Sanders D. B., Soifer B. T., 1990, *ApJ*, 362, 473

Tran H. D., Tsvetanov Z., Ford H. C., Davies J., Jaffe W., van den Bosch F. C., Rest A., 2001, *AJ*, 121, 2928

Tully R. B., 1988, *Nearby Galaxies Catalogue* (Cambridge University Press)

van Gorkom J., Schiminovich D., 1997, in Arnaboldi M., Da Costa G. S., Saha P., eds., *The Nature of Elliptical Galaxies*. ASP, San Francisco, p. 310

Watson D. M., Guptill M. T., Buchholz L. M., 1994, *ApJ*, 420, 21

Welch G. A., Sage L. J., 2003, *ApJ*, 584, 260

White R. L., Becker R. H., 1992, *ApJS*, 79, 331

Wiklind T., Henkel C., 2001, *A&A*, 375, 797

Wiklind T., Combes F., Henkel C., 1995, *A&A*, 297, 643

Wrobel J. M., Heeschen D. S., 1988, *ApJ*, 335, 677

Yi S. K., et al., 2005, *ApJL*, 619, L111

Young L. M., 2002, *AJ*, 124, 788

Young L. M., 2005, *AJ*, 634, 258

Young J. S., Xie S., Kenney J. D. P., Rice W. L., 1989, *ApJS*, 70, 699

Young J. S., Allen L., Kenney J. D. P., Lesser A., Rownd B., 1996, *AJ*, 112, 1903

Young J. S., Scoville N. Z., 1991, *ARA&A*, 29, 581

Yun M. S., Reddy N. A., Condon J. J., 2001, *ApJ*, 554, 803